ChemPhotoChem

Research Article
doi.org/10.1002/cptc.202400202

Chemistry Europe
European Chemical Societies Publishing

www.chemphotochem.org

Plasmonic Silver Nanoparticles Facilitate Electron Emission from Diamond upon Sun-Like Excitation

Alessandro Bellucci,[a] Matteo Mastellone,[a] Daniele Catone,[b] Patrick O'Keeffe,*[c] Faustino Martelli,[d] Giuseppe Ammirati,[b] Alessandra Paladini,[c] Stefano Turchini,[b] Francesco Toschi,[b] Antonio Santagata,[e] Maria Lucia Pace,[e] Riccardo Polini,[f] Raffaella Salerno,[e, f] Veronica Valentini,[a] and Daniele M. Trucchi[a]

The development of a stable, non-toxic material that emits electrons following absorption of visible light may have a major impact on the solar photocatalysis of difficult reactions such as CO_2 and N_2 reduction, as well as for targeted chemical transformations in general. Diamond is a good candidate, however it is a wide bandgap material requiring deep UV photons ($\lambda <$ 227 nm) to promote electrons from the valence band into the conduction band. Embedding silver nanoparticles under the diamond surface allows the photoconductivity of the diamond in the spectral region of the surface plasmon resonance to be increased, while also leading to an enhancement of visible light photoemission. Considering the low intensity of the light sources used in this work and the spectral properties of the enhanced photoconductivity and photoemission a mechanism based on plasmonically enhanced photoconductivity which in turn allows surface states emptied by photoemission to be recharged thus leading to enhanced photoemission in the visible range is proposed.

Introduction

Wide bandgap semiconductors, such as diamond, often have intriguing photoinduced properties that cannot be exploited by solar/visible light thus strongly limiting their use in applications. For example, the surface of hydrogen-terminated diamond has negative electron affinity (NEA)[1,2] which means that electrons excited into its conduction band in the vicinity of the surface are emitted without encountering a significant energy barrier from the surface both in vacuum[3] and in aqueous environments.[4] The efficient production of electrons from light has potentially a very wide range of applications in energy conversion,[5] photo(electro)catalysis,[4,6–9] water remediation,[10–12] and more. In general, to be viable for sustainable applications, a material needs to exploit a significant portion of the solar spectrum. However, diamond is a very wide bandgap material (5.47 eV), and so only absorbs light in the deep ultraviolet region of the spectrum thus limiting the practical application of diamond in solar-based devices.

Nonetheless, photoemission from diamond has been studied both with above[13] and below[14] bandgap excitation. Above the bandgap, photoemission experiments showed the feasibility of photoemission from diamond into both water and vacuum using UV light. It has also been demonstrated that below bandgap photoemission from diamond occurs but at orders of magnitude lower efficiency.[14] Different approaches have been attempted to render diamond capable of absorbing visible light by introducing sub-bandgap states, such as surface nanotexturing to form black diamond plates,[15–17] reactive ion etching,[18] inclusion of metallic nanoparticles[19,20] (NPs), doping by nitrogen,[21] phosphorous[22] or boron[21] and by using nanoparticles of diamond.[23] Nanodiamonds have also been used to demonstrate the photoactivity of suitably functionalized diamond under UV illumination leading to degradation of pollutants[24] and also under solar radiation by monitoring hydrogen production.[25]

Furthermore, AgNPs have been embedded in diamond deposited on both SiO_2[19] and Si[20] substrates. In the first case the AgNPs have been shown to have a variable plasmonic response depending on the synthesis details. In the case of the AgNPs in diamond on Si it was shown that the material has an increased photocatalytic efficiency for light with wavelengths $>$ 280 nm in the presence of AgNPs with respect to that

[a] A. Bellucci, M. Mastellone, V. Valentini, D. M. Trucchi
Istituto di Struttura della Materia-CNR (ISM-CNR), DiaTHEMA Lab, 00015 Monterotondo Scalo, Italy

[b] D. Catone, G. Ammirati, S. Turchini, F. Toschi
Istituto di Struttura della Materia (ISM), CNR, EuroFEL Support Laboratory (EFSL), Via del Fosso del Cavaliere 100, 00133 Roma, Italy

[c] P. O'Keeffe, A. Paladini
Istituto di Struttura della Materia (ISM), CNR, EuroFEL Support Laboratory (EFSL), 00015 Monterotondo Scalo, Italy
E-mail: patrick.okeeffe@ism.cnr.it

[d] F. Martelli
CNR-IMM, Area della Ricerca di Roma Tor Vergata, 100 Via del Fosso del Cavaliere, 00133 Rome, Italy

[e] A. Santagata, M. L. Pace, R. Salerno
Istituto di Struttura della Materia (ISM), CNR, Tito Scalo, FemtoLAB, C.da S. Loja, Zona Industriale, 85050 Tito Scalo Italy

[f] R. Polini, R. Salerno
Dipartimento di Scienze e Tecnologie Chimiche, Università di Roma "Tor Vergata", Via della Ricerca Scientifica 1, 00133 Roma, Italy

Supporting information for this article is available on the WWW under https://doi.org/10.1002/cptc.202400202

without. The authors suggested a mechanism involving emission of electrons into water followed by homogeneous catalysis.[20]

Another approach to photoemitting electrons with visible light[26–30] is to excite nanostructured plasmonic materials on their localized surface plasmon resonance (LSPR). In this case, there are a number of mechanisms that can be used to explain the emission, but they are generally based on non-linear processes involving multiphoton absorption,[28,29] or indeed, field emission effects.[30] These types of excitations generally require pulsed sources with peak intensities greater than 1 GW/cm^2. An exception to this was recently observed in photoemission from gold nanostars[31] where multiphotonic emission was observed with an CW source with sub MW/cm^2 intensities. However, at the intensity of the sun of 100 mW/cm^2, i.e. for solar applications, such processes are unlikely to occur and single photon linear processes dominate.

It is possible to increase the interaction between plasmonic NPs and semiconductors by embedding the nanoparticles into the semiconductor. The extensive body of research on this topic has been reviewed several times.[32–34] This approach has been used with some success on different wide band-gap photocatalysts such as TiO_2[35] and CeO_2[36] where, for example, gold and silver NPs have been used to induce energy transfer from visible light to the catalysts. The mechanisms that have been cited to explain the sensitization heavily depend on the relative energies of the plasmon resonance and the semiconductor bandgap.[33,37–40] In another example, it has recently been shown that by combining gold nanoparticles with diamond nanoparticles in aqueous suspensions it is possible to increase the emission of electrons into the surrounding water following visible light irradiation of the plasmon resonance of the gold nanoparticles with respect to bare diamond nanoparticles.[41]

In this work, we embed silver NPs inside diamond films in a manner similar to previous publications.[19,20] The novelty of this work lies in the association of the plasmonically enhanced photoconductivity to the enhanced photoemission and showing that these process occur even at the extremely low intensities comparable with the solar intensity. The knowledge gained will allow more efficiently emitting materials to be designed for solar applications.

Results and Discussion

A gallium focused ion beam combined with a field emission scanning electron microscope (Ga^+ FIB-FESEM) has been used to probe the depth and morphology of the Ag NPs which formed during the deposition of the CVD diamond layer onto the Ag layer during the fabrication of the AgNP@Dia sample (see methods for the details of the fabrication of the sample). The image shown in Figure 1(a) is taken following deposition of a Pt "strip" on the diamond surface followed by FIB milling of a trench into the surface of the sample. The difference in the brightness of the Pt, diamond and Ag allowed us to determine the depth of the Ag NPs giving a value of 410 ± 100 nm for the

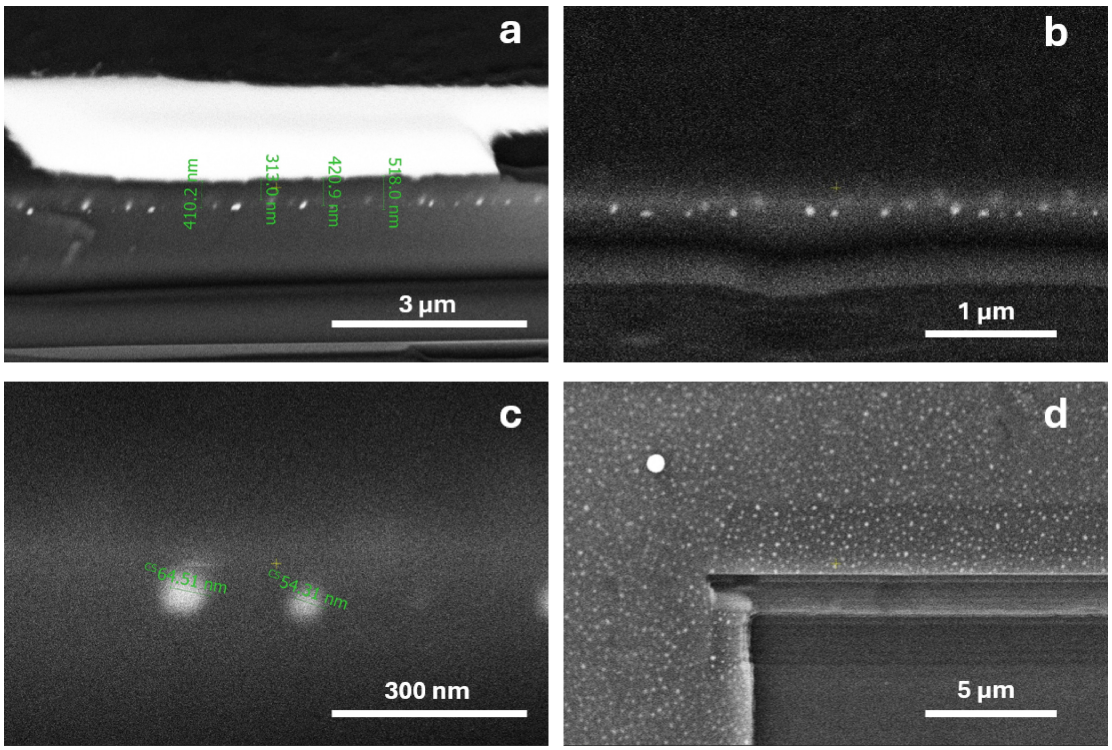

Figure 1. (a) SEM image on the AgNP@Dia sample performed by first depositing a Pt strip onto the surface of the sample then excavating a wedge-shaped hole into the surface of the sample and measuring a SEM image in cross section. (b, c) SEM images were taken in cross-section on a sample in which part of the diamond covering layer was removed by milling and viewing of the sample at 35° allowing the observation of embedded Ag nanoparticles (through the backscattered electrons) with varying levels of magnification, (d) same as the previous image but taken at 0° and observing a larger field (see text for details).

covering CVD diamond layer. A second series of images were taken by milling as much diamond as possible from the surface of the AgNP@Dia sample with out damaging the Ag NPs. Viewing the sample at 35° at different magnifications led to the images shown in Figures 1(b) and 1(c) (further images can be found in Figure S2 of the SI). These images show the presence of mainly spheroid and some ellipsoid shaped NPs with dimensions in the range of 45–65 nm. Finally an image (Figure 1(e)) was taken at an angle of 0° viewing a large area of the AgNP@Dia sample. This image shows a quite homogeneous distribution of the embedded Ag nanoparticles.

The Raman spectra of the AgNP@Dia sample and the diamond-on-diamond samples show the main peak at 1330 cm^{-1}, with a FWHM of ~4 cm^{-1}. This is compatible with the value measured for the pristine single-crystal commercial diamond substrate (before the deposition of the diamond overlayer) of 1332 cm^{-1}. A slight downshift of 2 cm^{-1} has been measured for both the samples with respect to the pristine sample, thus suggesting the presence of a small component of tensile stress due to the overlayer deposition beyond the Ag NPs presence.

The two narrow bands at 1459 and 1522 cm^{-1} indicate the presence of native defects in the pristine monocrystalline diamond.[42–46] Concerning the narrow (~5–6 cm^{-1}) bands centred at 1459 and 1522 cm^{-1}, Prawer et al.[43] showed that the sharpness of these peaks strongly suggests that their origin is in local, rather than extended, modes.[42,45] Here, they are directly attributable to local defects. Goss et al.[46] argue that 3H optical centres have been observed at 1506 and 1461 cm^{-1}, in good agreement with the bands centred at 1522 and 1459 cm^{-1} shown in Figure 1(b).

On the other hand, the main difference between the two spectra is the band at ~1129 cm^{-1}, which appears in the AgNP@Dia sample (see asterisk in Figure 2(a)). This peak was assigned to trans-PolyAcetilene (t-PA), which could be due to an increase in sp^2 defects in the AgNP@Dia sample or a SERS-like mechanism that increases this peak intensity.[44]

In order to further investigate the plasmonic nature of the embedded AgNPs we have performed an analysis of the optical transmittance and reflectance of the AgNP@Dia sample. The steady-state optical transmission of AgNP@Dia samples was measured using a homemade spectrometer with a 100 μm spot-size white-light source (see Figure 2(b)). In general, the absorption exhibits a clear peak at 2.25 eV with a width of 300 meV together with two less intense satellite peaks at 1.7 eV and 2.5–2.8 eV, respectively. No peak is visible in the pristine sample, indicating that the visible light absorption is due to the Ag NPs formed beneath the epitaxial diamond layer. The optical spectra exhibit a broad peak at 2.25 eV with two broad shoulders between 1.4–1.8 and 2.5–2.8 eV. The simulations

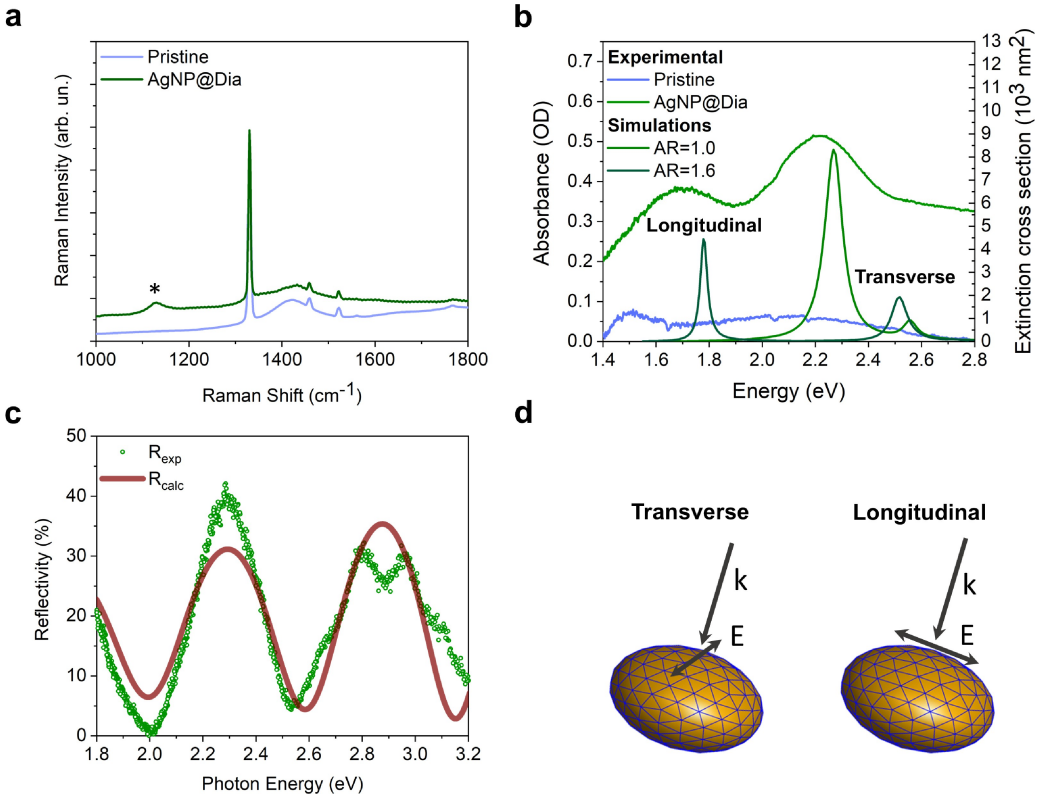

Figure 2. (a) Raman spectra of the pristine diamond and the AgNP@Dia sample. (b) Experimental steady-state optical transmission on the pristine diamond and AgNP@Dia samples together with simulations of the plasmonic response of AgNPs with varying morphology embedded in diamond. The asterisk indicates the enhanced band in the AgNP@Dia sample. (c) Steady-state reflectivity of the AgNP@Dia sample compared with a transfer matrix-based simulation of the oscillations due to constructive and destructive interference between reflections from the different interfaces within the sample. (d) Geometries depicting the direction of propagation of the light and electric field vectors in which the transverse and longitudinal plasmon resonances of the ellipsoid are excited.

(shown in Figure 2(b)) suggest that the broad peak at 2.25 eV is due to spherical particles which have only one plasmon resonance. The shoulders could be explained by ellipsoidal particles with aspect ratios in the range between 1 and 2. As an illustration, we show the simulated plasmon resonance of ellipsoids of Ag in diamond with aspect ratios of 1.6. The simulations show a longitudinal plasmon resonance in correspondence to the low-energy shoulder and a transverse plasmon resonance in the high-energy shoulder. These simulations agree with the microscopy measurements which show both spherical and ellipsoidal particles. Full details of the simulations can be found in the SI. Finally, the plasmonic nature of the absorption in the visible region is also confirmed by optical pump-probe time-resolved transmission measurements. In these experiments the sample was excited by light corresponding to the plasmon resonance and the dynamics of the relaxation process was monitored by measuring the change in transmission of the sample in the visible range over time. The temporal evolution of the induced absorption and bleaching are consistent with deexcitation of the plasmon resonance (see SI for a complete discussion).

The steady-state reflectivity measured in a similar fashion (see Figure 2(c)), also gives information on the geometry of the sample when combined with simulation. In this case, a Transfer Matrix method[47] was used to simulate the observed oscillations in the spectrum due to constructive and destructive interferences of the reflections from the different interfaces in the AgNP@Dia sample. The spectrum was simulated using an infinite diamond substrate, a 20 nm layer of material with dielectric constants averaged between Ag and Diamond, and a top layer of diamond. It should be noted that the simulations are not very sensitive to the thickness of the Ag/dia layer and the value of 20 nm was estimated from the nominal thickness of the Ag layer before dewetting. To match the observed reflectance spectrum a thickness of 415 nm was used for the covering layer. This is quite good agreement with the thickness extracted from the FESEM images discussed above.

Spectral photoconductivity measurements were then performed to derive the responsivity as a function of the impinging monochromatic radiation to demonstrate the photoelectronic action of the AgNPs in diamond. Figure 3(a) shows the responsivity (defined as the ratio between the collected photocurrent and the fluence of the lamp impinging on the sample) for the AgNP@Dia sample and the pristine sample. We found a significant increase of the responsivity in the 2.2–4.0 eV range, with a main peak around 2.65 eV. This enhancement in the collection of photoinduced charge carriers occurs in a confined range of wavelengths, which corresponds only partially to the wavelength range of the observed absorption peak. The enhanced sensitivity is peculiar for sub-bandgap photons since the pristine diamond shows a far flatter response for photon energies lower than 4 eV ($>$310 nm). The maximum responsivity is clearly reached at the diamond bandgap for both the samples. However, the higher value of responsivity at the bandgap for the AgNP@Dia sample is probably due to an enhanced capability of photocharge collection along the bulk caused by the presence of more conductive defects in this sample with respect to the pristine sample. Remarkably, the enhancement leads to a photoconductivity peak in the visible region, which is only one order of magnitude lower than the over-bandgap excitation. An important point to note here is that these measurements were performed with a weakly focussed monochromatised Xe lamp resulting in a light fluence of <2 mW/cm^2 in spectral regions not corresponding to peaks in the Xe lamp spectrum. Such an intensity is nearly 9 orders of magnitude lower than the threshold for even plasmonically enhanced non-linear processes observed in other systems[31] so we exclude the participation of non-linear processes in this case.

Having demonstrated the capability of AgNPs to promote charge carriers, it was necessary to perform an analysis on which type of charge carrier is excited. To confirm the role of the Ag NPs on the increase of the quantity of emitted photoelectrons, total photoemission current measurements were performed by irradiating the sample with selected monochromatic radiation. Figure 3(b) shows the photoemission current comparing the AgNP@Dia sample and the pristine diamond sample. We observe that the gain in the green region (532 nm, 2.33 eV) is close to 10 and reaches ~23 when the wavelength is in the blue region (405 nm, 3.06 eV). This finding agrees with the photoconductivity measurements, which show a sub-bandgap peak in the responsivity shifted towards shorter wavelengths with respect to the optical absorption peak (the absorption peak is at 2.2 eV while the photoconductivity peaks at 2.6 eV). Also in this case it is important to note that a weakly focussed low power continuous wave (CW) laser was used leading to fluences on the samples of 200 mW/cm^2. This is similar in intensity to the solar irradiance of 100 mW/cm^2 thus showing that the photoemission observed is relevant for solar applications and does not require high-fluence multiphoton processes to occur. Indeed, this intensity is nearly 7 orders of magnitude lower that that required to induce non-linear processes in the case of gold nanostars[31] so we can safely state that non-linear processes do not play a role here.

Combining these observations with information from the literature allows us to form a solid idea of the mechanism responsible for the emission of electrons from AgNP@Dia following absorption of visible light. Ristein et al.[3] showed that sub-bandgap photoemission is observed from hydrogen-terminated surfaces of single crystal diamond for photon energies as low as 2.0 eV, albeit with intensities orders of magnitude smaller than above-bandgap emission.[14] Initially, they suggested that this is due to the excitation of electrons from bulk defect states into the conduction band followed by diffusion to the surface and emission due to the NEA[1,2,48,49] characteristic of the hydrogenated surface.[48] More recently, they presented evidence that suggested that the sub-bandgap emission is, in fact, due to inhomogeneous emission from graphitic patches present on the diamond surface.[14] The emitted electrons effectively "see" the work function of the diamond and not that of the graphite (existing as a very small density of surface defects), thus effectively lowering the emission threshold.[14] This idea has been reproposed to explain electron emission following absorption of sub-bandgap radiation in a variety of

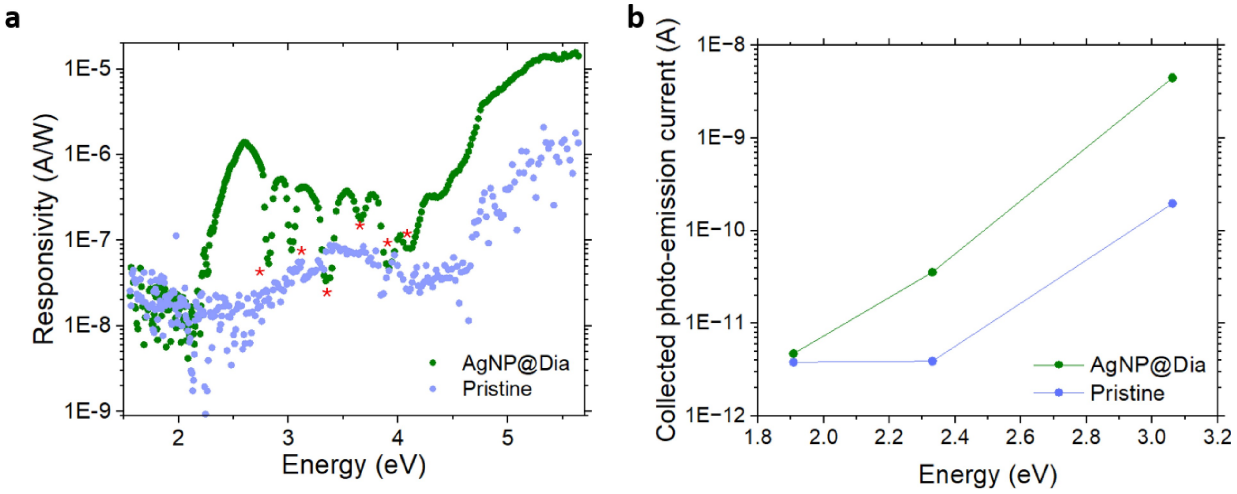

Figure 3. (a) Photoconductivity of pristine CVD diamond and AgNP@Dia as a function of photon energy showing the increase of photoconductivity in the visible range for AgNP@Dia. The asterisks indicate dips in the photoresponsivity spectrum due to artifacts introduced by the correction of the photoresponsivity for the Xe lamp intensity. (b) Photoemission current for pristine diamond and AgNP@Dia when photoexcited with three different continuous wave lasers of 650 nm (1.91 eV), 532 nm (2.33 eV), and 405 nm (3.06 eV) wavelengths.

systems such as nanodiamond-coated tungsten tips[50] (into vacuum) and suspensions of detonation nanodiamonds[23] (into water). In more recent works,[51,52] it has also been suggested that other occupied localized surface states on the C–H and C–OH terminations in both pristine and boron-doped diamond may also play a role in sub-bandgap excitation.

The main difference between the above systems and that proposed in this work is that our system presents two interfaces (Ag/Dia and Dia/Vacuum), which are spatially separated by 415 nm of CVD diamond. This point has important consequences for the underlying mechanism of electron emission. We first consider the 'buried' AgNP/Dia interface where the AgNPs-induced absorption of visible light takes place. We suggest that the increase in the photoconductivity could be due to excitation of the defect states at the AgNP/Dia interface. Similar defects have recently been shown to exist in polycrystalline CVD diamond, to give rise to unoccupied and occupied states within its bandgap, and to contribute to the transport of charges in the material.[53] Furthermore, increased sp^2 defectivity is a possible explanation for the appearance of an additional peak in the Raman spectra of the AgNP@Dia sample lending some experimental support to this idea. However, the peak in the photoconductivity of the AgNP@Dia is not only due to increased defectivity as this effect alone would give rise not to a peak, but to a tail of gradually lower intensity below the bandgap. The existence of a peak in the wavelength dependency of the photoconductivity suggests that visible-light absorption is enhanced by the presence of the LSPR of the AgNPs. Such enhanced absorption in the vicinity of plasmonic NPs has been extensively investigated and used to boost IR absorption in the surface enhanced IR absorption (SEIRA) method.[54,55] We suggest a similar mechanism is occuring here in which existing transitions within the semiconductor are boosted in intensity by the plasmonic NPs resulting in an increase of the absorption of the diamond in the vicinity of the LSPR. Such increased excitation must be combined with a transport mechanism through defects present in the CVD diamond to allow carrier transport from the Ag/Dia to the Dia/air interface. Therefore, the physical mechanism may involve sp^2-like defects in the diamond top layer, as transport paths leading electrons to the surface (see Figure 4(a) vs 4(b)).

Mechanisms we initially took into consideration were the internal photoemission of electrons from the AgNPs into the CB of the diamond, injection of hot electrons resulting from decay of the plasmon resonance into the diamond CB and excitation of electrons from filled defects at the AgNP/Dia interface into the diamond CB. Subsequently, these electrons in the CB could

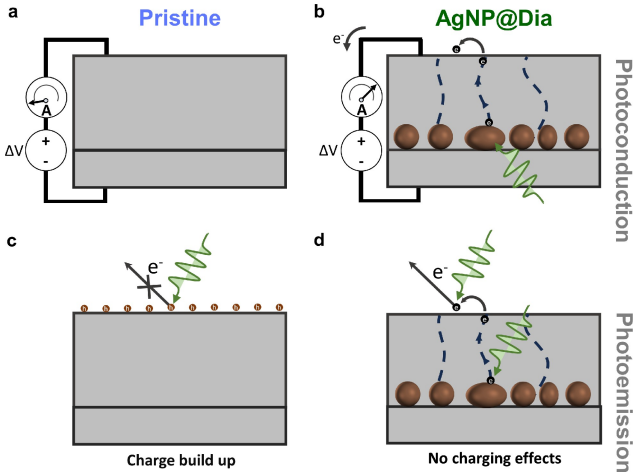

Figure 4. Illustration of the effects contributing to increased photoconductivity and photoemission in pristine diamond and AgNP@Dia. (a) The low-density defectivity of pristine diamond leads to low photoconductivity. (b) In AgNP@Dia the excitation of interface defects which subsequently increases the photoconductivity by hopping conduction through sp^2-like defects. (c) In pristine diamond surface photoemission from occupied localized surface states is frustrated due to the build-up of positive charge. (d) In AgNP@Dia the increased visible-light photoconductivity also leads also to increased visible-light induced photoemission by allowing the neutralization of the positive charges left behind by surface photoemission.

diffuse to the Dia/air (or vacuum) interface and be emitted thanks to the NEA of the hydrogen-terminated diamond. However, we exclude these mechanisms on an energetic basis as the initial excitation would require at least two photons which we have excluded on the basis of the very low intensity of the light sources used here. In fact, since the CVD diamond is intrinsic or even slightly p-type, the energy required to excite electrons into the CB is $> 1/2E_b$ leading to one photon cut-off at 2.74 eV, whereas we found that the peak of the observed increase in photoconductivity occurs at lower energy than this. As mentioned above, the measurements of photoconductivity and photoemission performed here were done with light intensities many orders of magnitude below the intensities where non-linear effects become prominent. Therefore, a more plausible explanation is that the increased photoconductivity serves only to refill electrons emitted from the diamond surface, in agreement with Ristein et al.[14], from small enclaves of graphitic-like defects on the surface.

Such emission would be frustrated by the build-up of positive charge on the surface of the diamond (see Figure 4(c)), while increased photoconductivity would reduce the build-up of positive charges and thus promote photoemission (see Figure 4(d)). We suggest that this is the mechanism through which the increased photoemission is observed at the LSPR of the AgNPs. The point to note is that this is a linear process as it does not require a multiphoton excitation of the electrons into the CB of the diamond and is therefore achievable also with low intensity CW sources as shown in the present work.

Conclusions

In summary, this work describes the incorporation of plasmonic Ag nanoparticles, with a size of about 50 nm, into a diamond matrix and shows how the resulting material emits electrons following illumination with low-intensity visible light with intensities comparable to that of the unconcentrated sun. Incorporation of the nanoparticles leads to a significant increase in the photoconductivity of the system in the 2.2–4.0 eV region and an increase of factors of 10 and 23 in the photoemission efficiency for photon energies of 2.34 and 3.06 eV, respectively. The low intensity of the light used in the measurements indicate a linear mechanism excluding a multiphoton internal emission of an electron from the silver into the conduction band of the diamond followed by diffusion to the surface and emission. Instead, we propose a mechanism involving plasmonically enhanced visible-light absorption by defect states at the Ag/Diamond interface which increases the photoconductivity of the material combined with photoemission from occupied surface states with electronic transport through defects. The understanding gained from these results will allow more efficiently emitting materials to be designed.

Experimental Section

Fabrication

An Ag layer with a nominal thickness of 10 nm was deposited by RF sputtering technique on a commercial single-crystal 3.0 x 3.0 x 0.3 mm^3 $<100>$ diamond plate (standard grade quality, produced by Element Six Ltd). Prior to deposition, the samples were cleaned with an oxidizing solution (1:1:1 proportion of boiling HNO_3:H_2SO_4:$HClO_4$). The Ag thin film was deposited at a base pressure of $\approx 2.0\times10^{-6}$ mbar, using an RF power of 250 W and a flow of Ar gas at the operating pressure of $\approx 1.0\times10^{-2}$ mbar. After the Ag deposition, the sample was transferred to a microwave plasma-enhanced CVD (MW-PACVD) system to deposit the upper diamond layer and heated at 500 °C at a base pressure of $\approx 5.0\times10^{-7}$ mbar. A microwave power of 1000 W was used for the deposition, which was carried out in two steps which differ in terms of gas fluxes (fixing the pressure at 40 Torr): 1) 30 min, using 200 standard cubic centimeters per minute (sccm) of H_2 flow and 3 sccm of CH_4 flow; 2) 2.5 h, using 200 sccm H_2 and 2 sccm CH_4 flows. The surface temperature was 740 ± 15 °C, as monitored by a two-color optical pyrometer. A final hydrogenation process with 200 sccm H_2 was performed for 10 min to ensure a hydrogen-terminated surface on diamond. The high temperature of the deposition process allows the formation of AgNPs and a homogenous coverage by a diamond film is obtained, where no surface anomalies are visible even with the NPs underneath (see SEM image in Figure S1).

FIB-FESEM

The Thermo Fisher Scientific SCIOS2 dual beam gallium focused ion beam combined with a field emission scanning electron microscope (Ga+ FIB-FESEM) instrument has been used to both cross-section the sample and get images of the sample both from above and in cross section. It has allowed us to clearly detect the presence of Ag nanoparticles embedded within the outermost diamond layer deposited by the CVD process as shown in Figure 1. The Ion Beam was set to 30 kV at currents of 300 pA and 30 pA which were able to perform a gross and fine milling of the sample, respectively. A eucentric working distance (WD) of 7.0 mm and a sample tilt of 52° were used to mill a trench of dimensions 20,15, 3 μm after a total of 35 minutes of FIB milling. Before performing the FIB milling a Pt "strip" was deposited onto the specimen which had the purpose of both better determining the position of the sample surface, thanks to the diverse brightness provided, for the Pt-Diamond layers, by the backscattered electrons, and protecting the latter during the FIB milling process. The Ga+ milling excavated material from one side of the Pt strip allowing us to determine the depth of the Ag NPs which, viewed with an angle of 35°, as reported in Figure 1(a), was of about 410 ± 100 nm.

Following this, another FIB milling excavation was performed with the aim of removing as little material as possible from the outermost CVD diamond layer to optimize the best FESEM parameters to be used for detecting the embedded Ag nanoparticles (through the backscattered electrons). The resulting images were taken in cross-section viewing of the sample at 35° (Figure 1(b), 1(c) and 1(d)) and successively by top viewing it at 0° (Figure 1(a)). The latter was acquired using the SCIOS2 FESEM with a setting that allows detection of the backscattered electrons through the whole range of accelerating voltages used. Figure 1(e) shows the homogeneous distribution of the embedded Ag nanoparticles obtained.

Raman Spectroscopy

Raman spectroscopy was carried out using a Horiba Scientific LabRam HR Evolution confocal spectrometer equipped with an Oxxius laser source ($\lambda = 532$ nm) and an XY-table, an electron-multiplier CCD detector, an Olympus U5RE2 microscope with 10× objective, and a grating with 600 grooves/mm. All Raman spectra were recorded from 1000 to 1800 cm^{-1} in the backscattering geometry, by focusing the 5 mW-beam on the sample and acquiring five spectra with an integration time of 5 s.

Steady-State Absorbance and Reflectivity

The steady-state absorbance and specular reflectivity were measured using a white light source generated by focusing 3 μJ of a 40 fs pulse of light centered at 800 nm into a CaF_2 crystal. The white light was then split into two equal parts and one part was focused to a spot with a diameter of 100 μm. The light transmitted and reflected were collected and analyzed in a spectrometer.

Spectral Photoconductivity

Spectral Photoconductivity has been performed by using monochromatic radiation produced by a Newport 74125 monochromator coupled to a Xe lamp. The beam passed through a collimating and focusing lens system, and through a SR540 Chopper (modulated at 14 Hz) before impinging on the sample. Metal contacts (two gold pads of 0.8 mm×2.8 mm with an intercontact distance of 1 mm) were deposited on the front surface and a gold pad (2.8 mm×2.8 mm) on the back surface ("sandwich" configuration for bulk measurements) of diamond plates and wire bonded to a printed circuit board for applying the bias voltage (500 V) and extracting the photogenerated current Iph. The photogenerated signal was collected by an EG&G Princeton Applied Research 5209 lock-in. The responsivity of the investigated samples is calculated as the ratio of Iph to incident lamp energy density and is reported in A/W for each wavelength (measured with a UV-Si photodetector Newport model 818-UV/DB).

Photoemission

Photoemission measurements were performed using CW lasers (650, 532, and 405 nm) with an output power fixed to 5 mW, The sample was positioned in a high vacuum chamber (base pressure of $\approx 1\times10^{-7}$ mbar) and an electric field of 100 V/cm was applied between the sample surface (using a metallic clip) and a metallic collector that allowed the illumination of the sample surface through a central hole (0.2 cm diameter). The geometry of the experimental setup is not fully optimized for maximizing the collection of photoelectrons (leading to a low yield), but it allows us to compare and demonstrate the performances of the different systems.

Simulations of the Optical Responses

Calculations of the plasmonic response of the AgNP@Dia system were performed using the MNPBEM toolbox.[56] Simulations of the oscillations in the reflection spectra were performed using the transfer matrix method.[47]

Acknowledgements

This paper has been supported by an Italian Ministerial grant PRIN PNRR 2022 Grant No. P2022ZHCT3 financed by the European Union – Next Generation EU. The authors express their gratefulness to Dr. Mauro Milazzo of Thermo Fisher Scientific – MSD, for his availability and support for the SCIOS2 FIB-SEM measurements. This research was conducted as part of the Infrastructure for LINKing Industry to Technologies – InLINK-IT" project (Regione Basilicata DD 15AB.2021/D.01143, CUP: G29J19001180003), funded under the ERDF Operational Program 2014–2020 – Action 1A.1.5.1. Public Notice "For the support of projects aimed at strengthening and expanding research infrastructures included in the Three-Year Research Infrastructure Plan of the Basilicata Region" DGR Basilicata N. 402–28th June 2019. Open Access publishing facilitated by Consiglio Nazionale delle Ricerche, as part of the Wiley - CRUI-CARE agreement.

Conflict of Interests

The authors declare no conflict of interest.

Data Availability Statement

The data that support the findings of this study are available from the corresponding author upon reasonable request.

Keywords: plasmonic nanoparticles · diamond · photoductivity · photoemission · solar photocatalysis

[1] F. Maier, J. Ristein, L. Ley, *Phys. Rev. B* **2001**, *64*, 165411.
[2] K. Tsugawa, H. Noda, K. Hirose, H. Kawarada, *Phys. Rev. B* **2010**, *81*, 045303.
[3] J. Ristein, W. Stein, L. Ley, *Phys. Rev. Lett.* **1997**, *78*, 1803.
[4] D. Zhu, L. Zhang, R. E. Ruther, R. J. Hamers, *Nat. Mater.* **2013**, *12*, 836.
[5] P. Calvani, A. Bellucci, M. Girolami, S. Orlando, V. Valentini, R. Polini, D. M. Trucchi, *Carbon* **2016**, *105*, 401.
[6] L. Zhang, R. J. Hamers, *Diamond Relat. Mater.* **2017**, *78*, 24.
[7] J. R. Christianson, D. Zhu, R. J. Hamers, J. R. Schmidt, *J. Phys. Chem. B* **2014**, *118*, 195.
[8] X. Xue, R. Chen, C. Yan, P. Zhao, Y. Hu, W. Zhang, S. Yang, Z. Jin, *Nano Res.* **2019**, *12*, 1229.
[9] C. J. M. van der Ham, M. T. M. Koper, D. G. H. Hetterscheid, *Chem. Soc. Rev.* **2014**, *43*, 5183.
[10] K. A. Rickman, S. P. Mezyk, *J. Adv. Oxid. Technol.* **2011**, *14*, 81.
[11] J. Raymakers, K. Haenen, W. Maes, *J. Mater. Chem. C* **2019**, *7*, 10134.
[12] R. Daily, D. Minakata, *Environ. Sci.: Water Res. Technol.* **2022**, *8*, 543.
[13] B. F. Bachman, D. Zhu, J. Bandy, L. Zhang, R. J. Hamers, *ACS Measurement Science Au* **2022**, *2*, 46.
[14] J. B. Cui, J. Ristein, L. Ley, *Phys. Rev. B* **1999**, *60*, 16135.
[15] A. Bellucci, M. Girolami, M. Mastellone, S. Orlando, R. Polini, A. Santagata, V. Serpente, V. Valentini, D. M. Trucchi, *Nanotechnology* **2020**, *32*, 024002.
[16] D. M. Trucchi, A. Bellucci, M. Girolami, P. Calvani, E. Cappelli, S. Orlando, R. Polini, L. Silvestroni, D. Sciti, A. Kribus, *Adv. Energy Mater.* **2018**, *8*, 1802310.
[17] M. Mastellone, A. Bellucci, M. Girolami, V. Serpente, R. Polini, S. Orlando, A. Santagata, E. Sani, F. Hitzel, D. M. Trucchi, *Nano Lett.* **2021**, *21*, 4477.

[18] P. Knittel, F. Buchner, E. Hadzifejzovic, C. Giese, P. Quellmalz, R. Seidel, T. Petit, B. Iliev, T. J. S. Schubert, C. E. Nebel, J. S. Foord, *ChemCatChem* **2020**, *12*, 5548.
[19] S. Li, J. Bandy, R. J. Hamers, *Diamond Relat. Mater.* **2018**, *89*, 190.
[20] S. Li, J. A. Bandy, R. J. Hamers, *ACS Appl. Mater. Interfaces* **2018**, *10*, 5395.
[21] S. Choudhury, R. Golnak, C. Schulz, K. Lieutenant, N. Tranchant, J.-C. Arnault, M.-A. Pinault-Thaury, F. Jomard, P. Knittel, T. Petit, *C* **2021**, *7*, 28.
[22] A. Gorbachev, A. Vikharev, A. Afanasiev, A. Vikharev, I. Bandurkin, D. Radishev, M. Drozdov, S. Bogdanov, *Vacuum* **2023**, *215*, 112335.
[23] F. Buchner, T. Kirschbaum, A. Venerosy, H. Girard, J.-C. Arnault, B. Kiendl, A. Krueger, K. Larsson, A. Bande, T. Petit, C. Merschjann, *Nanoscale* **2022**, *14*, 17188.
[24] W. A. Maza, V. M. Breslin, T. I. Feygelson, P. A. DeSario, B. B. Pate, J. C. Owrutsky, A. Epshteyn, *Appl. Catal. B* **2023**, *325*, 122306.
[25] C. Marchal, L. Saoudi, H. A. Girard, V. Keller, J.-C. Arnault, *Adv. Energy Sustain. Res.* **2024**, *5*, 2300260.
[26] A. Al-Zubeidi, B. Ostovar, C. C. Carlin, B. C. Li, S. A. Lee, W.-Y. Chiang, N. Gross, S. Dutta, A. Misiura, E. K. Searles, A. Chakraborty, S. T. Roberts, J. A. Dionne, P. J. Rossky, C. F. Landes, S. Link, *Proceedings of the National Academy of Sciences* **2023**, *120*, e2217035120.
[27] D. Solti, K. D. Chapkin, D. Renard, A. Bayles, B. D. Clark, G. Wu, J. Zhou, A.-L. Tsai, L. Kürti, P. Nordlander, N. J. Halas, *J. Am. Chem. Soc.* **2022**, *144*, 20183.
[28] P. Jiang, W. Zheng, X. Li, L. Zhang, Y. Liu, Y. Wang, Y. Li, Y. Gao, H. Yang, Y. Liu, Q. Gong, C. Wu, *Nano Lett.* **2023**, *23*, 7327.
[29] D. Novko, V. Despoja, M. Reutzel, A. Li, H. Petek, B. Gumhalter, *Phys. Rev. B* **2021**, *103*, 205401.
[30] S. Zhou, K. Chen, M. T. Cole, Z. Li, J. Chen, C. Li, Q. Dai, *Adv. Mater.* **2019**, *31*, 1805845.
[31] M. Sivis, N. Pazos-Perez, R. Yu, R. Alvarez-Puebla, F. J. García de Abajo, C. Ropers, *Communications Physics* **2018**, *1*, 13.
[32] D. Catone, L. D. Mario, F. Martelli, P. O'Keeffe, A. Paladini, J. S. P. Cresi, A. K. Sivan, L. Tian, F. Toschi, S. Turchini, *Nanotechnology* **2020**, *32*, 025703.
[33] K. Wu, J. Chen, J. R. McBride, T. Lian, *Science* **2015**, *349*, 632.
[34] C. Clavero, *Nat. Photonics* **2014**, *8*, 95.
[35] D. C. Ratchford, A. D. Dunkelberger, I. Vurgaftman, J. C. Owrutsky, P. E. Pehrsson, *Nano Lett.* **2017**, *17*, 6047.
[36] J. S. Pelli Cresi, M. C. Spadaro, S. D'Addato, S. Valeri, S. Benedetti, A. Di Bona, D. Catone, L. Di Mario, P. O'Keeffe, A. Paladini, G. Bertoni, P. Luches, *Nanoscale* **2019**, *11*, 10282.
[37] A. Furube, S. Hashimoto, *NPG Asia Mater.* **2017**, *9*, e454.
[38] B. Brady, V. Steenhof, B. Nickel, A. M. Blackburn, M. Vehse, A. G. Brolo, *ACS Appl. Energ. Mater.* **2019**, *2*, 2255.
[39] N. Wu, *Nanoscale* **2018**, *10*, 2679.
[40] S. K. Cushing, J. Li, F. Meng, T. R. Senty, S. Suri, M. Zhi, M. Li, A. D. Bristow, N. Wu, *J. Am. Chem. Soc.* **2012**, *134*, 15033.
[41] S. Orlanducci, G. Ammirati, A. Bellucci, D. Catone, L. C. Gontard, F. Martelli, R. Matassa, A. Paladini, F. Toschi, S. Turchini, P. O'Keeffe, *ACS Appl. Opt. Mater.* **2024**, *2*, 1180.
[42] S. Prawer, K. Nugent, D. Jamieson, *Diamond Relat. Mater.* **1998**, *7*, 106.
[43] S. Prawer, I. Rosenblum, J. Orwa, J. Adler, *Chem. Phys. Lett.* **2004**, *390*, 458.
[44] T. López-Ríos, E. Sandré, *J. Raman Spectrosc.* **1998**, *29*, 733.
[45] J. O. Orwa, K. W. Nugent, D. N. Jamieson, S. Prawer, *Phys. Rev. B* **2000**, *62*, 5461.
[46] J. P. Goss, B. J. Coomer, R. Jones, T. D. Shaw, P. R. Briddon, M. Rayson, S. Öberg, *Phys. Rev. B* **2001**, *63*, 195208.
[47] K. J. Pascoe, Reflectivity and Transmissivity through layered lossy media: A user-friendly approach, Technical Report AFIT/EN-TR-01-07, Air-Force Institute of Technology, Wright Patterson Air Force base, Ohio, Wright Patterson Air Force base, Ohio **2001**.
[48] J. B. Cui, J. Ristein, L. Ley, *Phys. Rev. Lett.* **1998**, *81*, 429.
[49] F. J. Himpsel, J. A. Knapp, J. A. VanVechten, D. E. Eastman, *Phys. Rev. B* **1979**, *20*, 624.
[50] A. Tafel, S. Meier, J. Ristein, P. Hommelhoff, *Phys. Rev. Lett.* **2019**, *123*, 146802.
[51] M. Sobaszek, M. Brzhezinskaya, A. Olejnik, V. Mortet, M. Alam, M. Sawczak, M. Ficek, M. Gazda, Z. Weiss, R. Bogdanowicz, *Small* **2023**, *19*, 2208265.
[52] A. Chemin, I. Levine, M. Rusu, R. Vaujour, P. Knittel, P. Reinke, K. Hinrichs, T. Unold, T. Dittrich, T. Petit, *Small Methods* **2023**, *7*, 2300423.
[53] T. Dittrich, S. Fengler, *Semicond. Sci. Technol.* **2022**, *38*, 015015.
[54] M. Janneh, *Res. Optics* **2022**, *6*, 100201.
[55] T. G. Mayerhöfer, S. Pahlow, J. Popp, *Nat. Photonics* **2020**, *9*, 741.
[56] J. Waxenegger, A. Trügler, U. Hohenester, *Comput. Phys. Commun.* **2015**, *193*, 138.

Manuscript received: June 3, 2024
Revised manuscript received: October 18, 2024
Accepted manuscript online: October 27, 2024
Version of record online: November 28, 2024